Tree-ring cellulose $\delta^{18}O$ records similar large-scale climate influences as precipitation $\delta^{18}O$ in the Northwest Territories of Canada

FIELD R.D.[1,10*]; ANDREU-HAYLES L.[2,3,4,10*]; D'ARRIGO R.D.[2], OELKERS R.[2], LUCKMAN B.H.[5], MORIMOTO D.[5], BOUCHER E.[6], GENNARETTI F.[7], HERMOSO I.[6], LAVERGNE A.[8], LEVESQUE M.[9]

[1]NASA Goddard Institute for Space Studies, Columbia University Dept. Applied Physics and Applied Mathematics, New York, NY, U.S.A.

[2] Tree-Ring Laboratory, Lamont-Doherty Earth Observatory of Columbia University, Palisades, NY, 10964, U.S.A.

[3]CREAF, Bellaterra (Cerdanyola del Vallés), Barcelona, Spain.

[4]ICREA, Pg. Lluís Companys 23, Barcelona, Spain.

[5] Department of Geography, University of Western Ontario, London, Canada.

[6]Department of Geography, GEOTOP, University of Québec at Montréal, Canada.

[7]Institut de Recherche sur les Forêts, Groupe de Recherche en Écologie de la MRC d'Abitibi, UQAT, Amos, Québec, J9T 2L8, Canada.

[8]Carbon Cycle Research Group, Space and Atmospheric Physics, Department of Physics, Imperial College London, London, SW7 2AZ, UK.

[9]Forest Management Group, Department of Environmental Systems Science, ETH Zurich, 8092 Zurich, Switzerland.

[10]These authors contributed equally: Robert D. Field, Laia Andreu-Hayles

*Corresponding authors: robert.field@columbia.edu; lah@ldeo.columbia.edu.

Abstract

Stable oxygen isotopes measured in tree rings are useful for reconstructing climate variability and explaining changes in physiological processes occurring in forests, complementing other tree-ring parameters such as ring width. Here, we analyzed the relationships between different climate parameters and annually resolved tree-ring $\delta^{18}O$ records ($\delta^{18}O_{TR}$) from white spruce (*Picea glauca* [Moench]Voss) trees located near Tungsten (Northwest Territories, Canada) and used the NASA GISS ModelE2 isotopically-equipped general circulation model (GCM) to better interpret the observed relationships. We found that the $\delta^{18}O_{TR}$ series were primarily related to temperature variations in spring and summer, likely through temperature effects on the precipitation $\delta^{18}O$ in spring, and evaporative enrichment at leaf level in summer. The GCM simulations showed significant positive relationships between modelled precipitation $\delta^{18}O$ over the study region and surface temperature and geopotential height over northwestern North America, but of stronger magnitudes during fall-winter than during spring-summer. The modelled precipitation $\delta^{18}O$ was only significantly associated with moisture transport during the fall-winter season. The $\delta^{18}O_{TR}$ showed similar correlation patterns to modelled precipitation $\delta^{18}O$ only during spring-summer when water matters more for trees, with significant positive correlations with surface temperature and geopotential height, but no correlations with moisture transport. Overall, the $\delta^{18}O_{TR}$ records for northwestern Canada reflect the same significant large-scale climate patterns as precipitation $\delta^{18}O$ for spring-summer, and therefore have potential for reconstructing past atmospheric dynamics in addition to temperature variability in the region.

Keywords: paleoclimate, stable isotopes, dendrochronology, general circulation models, NASA GISS Model E2, snow

Declarations

Funding

This research was supported by a Lamont-Doherty Earth Observatory Climate Center grant and by US National Science Foundation (NSF) grants PLR-1504134, PLR-1603473, AGS-1502150 and OISE-1743738.

Conflicts of interest/Competing interests

The authors have no relevant financial or non-financial interests to disclose.

Availability of data and material

The data that support the findings of this study are available from the ITRDB database at the NOAA server (link) and Arctic Data Center (ADC).

Code availability

All code will be made publicly available should the paper be accepted for publication.

Authors' contributions

R.D.F and L.A-H design the study, conducted the analyses and wrote the manuscript with contributions from all authors. B.H.L and D.M collected the samples and generated the reference tree-ring width chronology. L.A-H and R.O. generated the isotopic chronology at the Lamont-Doherty Earth Observatory of Columbia University.

Ethics approval

This paper is in compliance with Ethical Standard

Consent to participate

All authors consent to participate in this paper.

Consent for publication

All authors consent for publication of the submitted manuscript

1. Introduction

Tree rings have been used to reconstruct climate, particularly temperature, over northwestern North America prior to the instrumental period, primarily using tree-ring width (TRW) and maximum latewood density (MXD) data for the past millennium (Anchukaitis et al. 2012; Briffa et al. 2004; D'Arrigo et al. 2014). Such records have also been used to generate indices of patterns of large-scale atmospheric-ocean circulation, such as the Aleutian Low, or the Pacific Decadal Oscillation (PDO) for the north Pacific sector (e.g. D'Arrigo et al. 2001; Gaglioti et al. 2019; Villalba et al. 2011). Tree-ring density proxies such as MXD have been shown to have a more stable and robust temperature signal than ring-width chronologies from the same trees, and thus have been used to generate temperature reconstructions for a variety of northern sites, e.g. in British Columbia (Wilson and Luckman 2003), at latitudinal treeline at Firth River in Alaska (Anchukaitis et al. 2012; Andreu-Hayles et al. 2011a) and in the Yukon (Morimoto 2015), as well as for the Northern Hemisphere (Anchukaitis et al. 2017; Wilson et al. 2016). Blue intensity (BI), a novel proxy for density, has been used to produce reconstructions in Yukon (Wilson et al. 2019) and the Gulf of Alaska (Wilson et al. 2017), among other locations.

The isotopic composition of stable oxygen ($\delta^{18}O$, ratio of ^{18}O to ^{16}O relative to a standard) measured in tree rings can be used as another climate proxy and can provide complementary and unique information relative to TRW and MXD/BI data. This isotopic information includes, for example, physiological insights into tree response to environmental changes in boreal and other terrestrial ecosystems (e.g. Andreu-Hayles et al. 2011b; Barber et al. 2000; Levesque et al. 2017), information about the source water used by the tree (e.g. Gessler et al. 2014; McCarroll and Loader 2004), and climate variability (e.g. Andreu-Hayles et al. 2017; Gennaretti et al. 2017). The $\delta^{18}O$ signature recorded in tree rings mostly results from 1) the isotopic composition of the source water that is taken up by the roots; 2) the isotopic enrichment occurring due to leaf transpiration; and 3) the isotopic exchange between oxygen atoms between cellulose and xylem water when cellulose is formed. The first and the third contributions are related to the water source signal of precipitation $\delta^{18}O$ and isotopic balance in the soil (Dansgaard 1964). Precipitation $\delta^{18}O$ can vary regarding the trajectory of the air masses, the distance from the original source and their exposure to warmer/colder atmospheric conditions that will determine the amount of moisture that can be held and the number of rainouts (i.e. depleting the original

$\delta^{18}O$ signature) before arriving to the studied trees. The $\delta^{18}O$ of source water can also vary due to the use of water pools from different soil depths (Barbeta et al. 2020; Brinkmann et al. 2018). The second contribution, the enrichment due to leaf transpiration, is associated to physiological response of the plant to changes in relative humidity and temperature, both determining vapor pressure deficit (VPD). Finally, post photosynthetic fractionation can also occur (Gessler et al. 2014) modulating the $\delta^{18}O$ signal recorded in tree-rings. Although the mechanisms described above are well accepted, there are strengths and caveats on their physiological interpretation (Barbour 2007; Cernusak et al. 2016; Gessler et al. 2014). Disentangling the dominant signal in cellulose $\delta^{18}O$, leaf water enrichment or source water isotopic signal, can be challenging.

Because tree-ring $\delta^{18}O$ ($\delta^{18}O_{TR}$) records are affected by climate, they can be a powerful additional proxy for reconstructing atmospheric circulation patterns for centuries prior to the instrumental period (Balting et al. 2021; Szejner et al. 2016). Understanding the linkages between $\delta^{18}O_{TR}$ and precipitation $\delta^{18}O$ is also important for improving past climate reconstructions in these high-latitude boreal regions (Anchukaitis et al. 2017; D'Arrigo et al. 2014; Wilson et al. 2016). In the extratropical regions of the Northern Hemisphere, precipitation $\delta^{18}O$ is strongly related to temperature (Birks and Edwards 2009). This relationship is in part reflected in the positive correlations typically seen between $\delta^{18}O_{TR}$ and temperature, and in theory may be attributable to large-scale atmospheric circulation patterns that prevail in this area. For example, summer temperatures were reconstructed over the last millennium using $\delta^{18}O_{TR}$ records (Naulier et al. 2015), and annual temperatures and $\delta^{18}O$ meteoric water values were estimated from Pleistocene subfossil wood from Bylot Island, Canada (Csank et al. 2013). In the southern Yukon, an atmospheric general circulation model equipped with stable water isotope tracers demonstrated that high $\delta^{18}O$ values in meteoric water were associated with an intensified Aleutian Low pressure cell, bringing stronger southerly moisture flow to eastern Alaska and the southern Yukon (Field et al. 2010). Such general circulation models can provide an idealized picture of the climatic influence on local precipitation $\delta^{18}O$ (Field et al. 2010; Porter et al. 2014) in the absence of long-term precipitation $\delta^{18}O$ records.

Determination of the climate signal in $\delta^{18}O_{TR}$ requires comparisons with observed climate variables, typically obtained from nearby meteorological stations. In prior work, Begin et al.

(2015) and Naulier et al. (2015) identified summer maximum temperature and VPD influences on black spruce $\delta^{18}O_{TR}$ for a site in north-central Quebec using weather station data from three stations 100-300 km away, each with data available for roughly 50 years. Holzkämper et al. (2012) reported a robust relationship between spring temperature and precipitation with white spruce $\delta^{18}O$ at a site in Nunavut over the 1986-2004 interval for a weather station roughly 300 km away. Csank et al. (2016) documented spring/summer climatic controls on $\delta^{18}O$ using Global Historical Climate Network (GHCN) stations within 100 km of sampling sites in south-coastal Alaska between 1949 and 2011.

Station records are typically few, very limited across space and have short or incomplete records in remote regions such as those studied herein (e.g. Holzkamper et al. 2012), making it difficult to identify robust local or large-scale climatic influences. Gridded observational products and meteorological reanalysis are, in theory, an alternative, and can also help to identify regional influences on tree-ring signals. For example, gridded climate products have been used for reconstructing summer temperatures (Gennaretti et al. 2017) and streamflow (Brigode et al. 2016) in northern Quebec.

Here, our objective is to assess the climate signal and atmospheric circulation patterns associated with inter-annual variations in a newly-developed alpha-cellulose-derived $\delta^{18}O_{TR}$ chronology for a site located in the Northwest Territories, Canada and thus determine the potential of these records to reconstruct large-scale climate variability in the region. We focus specifically on how these relationships are detected in several different types of datasets, namely: (i) homogenized station records and 'raw' station records with additional parameters, (ii) two gridded temperature datasets estimated from meteorological station data but using different interpolation techniques, and (iii) a meteorological reanalysis product. We also use an isotopically-equipped general circulation model (GCM) to understand climatic controls on local precipitation $\delta^{18}O$, and to help interpret the different seasonal relationships identified between $\delta^{18}O_{TR}$ and the climate observations. Overall, we aimed to determine the potential of using tree-ring $\delta^{18}O$ to reconstruct large-scale climate indicators interpreting what climatic signals might be detectable using a broad range of data and GCM simulations. Our interest in this region is motivated by the need to provide context prior to the instrumental period for north Pacific climate variability and high-latitude climate change.

2. Data and methods

2.1. Tree-ring data

The tree-ring samples were collected from white spruce (*Picea glauca* [Moench]Voss) located at 1145 m a.s.l near Tungsten (61.98ºN; -128-25ºW; Figure 1), Northwest Territories (NWT), Canada in the year 2003 (Morimoto, 2015). The sampled stand consisted of isolated tall spruce trees growing from an underbrush of willow (*Salix* spp.) and alder (*Alnus* spp.) on an irregular, 10-15° north- east facing slope about 100 m below the contiguous treeline. A total of 26 tree-ring samples (5 mm-cores) from 25 trees were selected from the "Western Collection", a tree-ring data set that was donated by Brian Luckman from the University of Western Ontario to the Tree-Ring Lab at the Lamont-Doherty Earth Observatory (LDEO) and University of Saint Andrews, UK.

The samples were scanned at a resolution of 3200 dpi using a color calibrated Epson V850 Pro scanner and the SilverFast Ai IT8 imaging software (Version 8) and the TRW were measured using the software Coorecorder 9.3 (Cybis Electronik 2019). Ring width was measured to 0.001mm (.0038px) precision and cross-dated against the original chronology (Morimoto 2015) to ensure accurate calendar dating using dendrochronological methods (Stokes and Smiley 1968). The 26 individual ring-width timeseries were standardized using a 200-year spline (Cook and Peters 1981) after applying a power transformation to stabilize the variance (Cook and Peters 1997). An autoregressive model was then applied to the individual standardized ring-width series to create residual ring-width timeseries. These were averaged using a robust mean with the software Arstan (Cook and Kairiukstis 1990) resulting in TRW residual chronology that emphasizes high-frequency variability.

The $\delta^{18}O$ records were generated at LDEO following the technique described in Andreu-Hayles et al. (2019) for cellulose extraction and the measurement of $\delta^{18}O$ using high-temperature pyrolysis in a High Temperature Conversion Elemental Analyzer (TC/EA) coupled to a Thermo Delta plus mass spectrometer. Five trees were analyzed from 1900 to 2003, a period that overlaps partially with the climate data. We selected one core sample from five individual trees mostly based on the following criteria: (1) high correlations with the master TRW chronology to be sure that they were representative of the stand; (2) trees older than 200 years to avoid potential juvenile effects; (3) visually adequate samples for wood preparation (e.g. wide rings for cutting, no locally absent rings or signs of reaction wood). Each ring was separated under a stereomicroscope using a scalpel and was analyzed individually. The resulting annual timeseries from the five individual trees were normalized and the resulting z-scores were averaged to compute a mean chronology. The Expressed Population Signal (EPS) metric was also calculated as a metric of the level of agreement among the individual trees. An EPS value exceeding the widely used threshold value of 0.85 (Wigley et al. 1984) indicates a high level of agreement among trees.

2.2. Climate data and the NASA ModelE2 isotopically-equipped climate model

We used climate data from different sources, including individual station records nearest to the study site and gridded products, each constructed differently, and which allow us to identify regional relationships between climate parameters and the tree-ring data beyond what can be detected for a single weather station. The gridded products were:

1. GHCN: The Global Historical Climate Network (Durre et al. 2010) is a standard, quality-controlled and corrected station-based dataset with daily and monthly resolution. GHCN has temperature, precipitation, and snow-depth data, but no humidity data. Data were available from 1938-2002 for the Watson Lake A station, shown in Figure 2. Most data were missing from October 1993 to December 1994 and snow depth records began in 1956.

2. ISD: The National Centers for Environmental Information Integrated Surface Database (Smith et al. 2011) contains hourly records compiled from operational weather stations, with a more complete list of variables than GHCN. Daily maximum temperature was computed from hourly observations, and maximum daily vapor-pressure deficit (VPDMAX) was calculated from temperature and dew point temperature, which was not available in the GHCN. The data for Watson Lake were only available from July 1977 to 2002, but had good record availability during the October 1993 to December 1994 period missing from the GHCN archive for this site.

3. GISTEMP: The Goddard Institute for Space Studies dataset (Lenssen et al. 2019) is a gridded product of mean surface temperature (T_{surf}) anomalies going back to 1880, aggregated from different station datasets, including the GHCN. There is limited spatial interpolation, so there are large areas of missing data and higher uncertainties going back further in time.

4. BEST: The Berkeley Earth Surface Temperature dataset (Rohde et al. 2013) is a gridded product based on different station data going back to 1850, also including GHCN. The underlying data are subject to sophisticated quality control and cross-checking and there are separate estimates of mean daily maximum temperature (TMAX), daily minimum temperature (TMIN) and daily average temperature (TAVG) estimates. The BEST temperature fields are smoother than GISTEMP because of broader spatial interpolation over regions of missing station data.

5. UDEL precipitation: The University of Delaware global gridded precipitation product (Legates and Willmott 1990) is a spatially interpolated dataset derived from various sources of gauge data, starting with the GHCN and supplemented from other sources where GHCN data are sparse. The version 3.01 version used here is described at http://climate.geog.udel.edu/~climate/html_pages/Global2011/README.GlobalTsP2011.html

6. Atmospheric Reanalyses: Reanalyses products provide a complete estimate of the state of the atmosphere by combining a numerical weather prediction model and observations from different sources. This allows us to examine metrics other than surface variables such as large-scale circulation features. In our case, we examine relationships with horizontal moisture flux, defined as the product of specific humidity (q) and the vector wind field <u,v> in the mid troposphere to identify possible source water pathways, sea-level pressure, and geopotential height (Z) in the mid-troposphere to identify possible large-scale circulation influences. Reanalyses are less suitable for analyzing local climate-tree ring relationships but are the only practical means of identifying large-scale circulation influences. We used two reanalysis products to guard against product-specific interpretation of our analysis. The National Center for Environmental Prediction / National Center for Atmospheric Research reanalysis (Kalnay et al. 1996) is a mature, coarse-

resolution reanalysis going back to 1948, providing coverage for approximately half the tree-ring record, and which assimilates a broad range of surface, upper air and satellite data. For comparison, we also used the Twentieth Century Reanalysis System version 3 product (20CRv3, Slivinski et al. 2019). 20CRv3 provides coverage for the entire tree-ring record but is constrained only by surface pressure observations.

The NASA GISS ModelE2: The ModelE2 GCM (Schmidt et al. 2014) is one of several GCMs equipped with stable water isotope tracers. The simulations are forced by observed, interannually-varying Sea Surface Temperatures (SSTs). Model output can be used to identify idealized climate controls on the isotopic composition of precipitation $\delta^{18}O$ over a region of interest and examine idealized relationships between climate patterns and precipitation $\delta^{18}O$ for seasons outside of the growth season.

2.3 Data analyses

We examined correlations between the Tungsten $\delta^{18}O_{TR}$ data and the aforementioned climate datasets. All of them span different periods and are constructed differently. We filtered the climate data seasonally, with the expectation that climate relationships would be most strongly affected by interannual variability during the growing season. The $\delta^{18}O_{TR}$ could also be influenced by climate during the previous winter due for example to snow $\delta^{18}O$, spring runoff, and consequently soil moisture available for the growth season, considering that during winter the climatic influence on high-latitude precipitation $\delta^{18}O$ is more pronounced (Birks and Edwards 2009; Field et al. 2010). Large-scale climatic influences were also expected to vary seasonally because of their distinct strengths during different seasons, for example the Aleutian Low which is most strongly expressed in winter (Hartmann and Wendler 2005).

We compared the relationships of precipitation $\delta^{18}O$ with large-scale climate provided by the ModelE2 GCM versus the relationships of $\delta^{18}O_{TR}$ with the same climate variables from re-analyses products. This comparison can help us to determine the prevailing signal in $\delta^{18}O_{TR}$ that results from strong climate influences on both $\delta^{18}O$ composition of soil water and tree physiological processes.

3. Results

3.1. Tree-ring chronologies

The Tungsten TRW chronology spans from 1584 to 2002, although replication is lower for the earlier period. EPS values in the ring widths (N=25 trees, 26 timeseries) and $\delta^{18}O_{TR}$ (N=5) chronologies (Figure 2) exceed 0.85 from 1900 to 2002, suggesting that both tree-ring chronologies can be considered reliable for the studied period. The average of the Pearson correlation coefficient values (r) between each tree timeseries was 0.601 ($p < 0.05$; 1900-2003), 0.68 ($p < 0.05$; 1900-1969) and 0.513 ($p < 0.05$; 1970-2003), while the mean of the $\delta^{18}O_{TR}$ values was 19.02 ±0.77 ‰ (1900-2003), 19.08 ±0.67 ‰ (1900-1969) and 18.88 ±0.98 ‰ (1970-2003). Thus, lower correlations among trees and higher Standard Deviation (SD) were found during the period 1970-2003 (r = 0.513, $p < 0.05$ and SD = 0.98 ‰) than during the period 1900-1969 (r = 0.68, $p < 0.05$ and SD = 0.68 ‰). This less common variance and higher variability among trees is also shown by the lower SD of the $\delta^{18}O_{TR}$ chronology (z-scores) in the period 1970-2003 (SD = 0.58) than in the period 1900-1960 (SD = 0.49).

3.2. Observed climate relationships of tree ring width and $\delta^{18}O$

Table 1 lists the Pearson's correlation coefficients between the residual TRW chronology and several climate variables for different seasons and periods of observational data availability. Over the 1977-2002 period common to both the ISD and GHCN gridded datasets, TRW was negatively correlated to spring (MAM) minimum temperature using both ISD (r=-0.48, $p < 0.05$) and GHCN (r=-0.49, $p < 0.05$), and positively correlated to snow depth (SNDP, r=0.64, $p < 0.05$). The relationship of TRW with TMIN and SNDP were not significant over the longer 1938-2002 period, although there was a weak positive correlation (r = 0.34, $p < 0.05$) with summer (JJA) TMAX, and weak negative correlations with precipitation for seasons prior to the growing period, peaking at r = -0.39 for winter-spring-summer (previous DJFMAMJJA).

Table 2 lists the Pearson's correlation coefficients between the $\delta^{18}O_{TR}$ and these same climate variables. VPDMAX and TMAX were positively correlated during the MAMJJA period (r=-0.86, $p < 0.05$) and both agreed with $\delta^{18}O_{TR}$ z-scores fluctuations (Figure 3). The $\delta^{18}O_{TR}$ z-scores showed a strong correlation with average spring-summer TMAX (Figure 3a) from the GHCN dataset for 1938-2002 (MAMJJA, $r = 0.67$, $p < 0.01$) but lower correlation over the 1977-2002 period using TMAX from the ISD dataset (MAMJJA, $r = 0.49$, $p < 0.05$). This correlation with the spring-summer ISD TMAX was lower than when $\delta^{18}O_{TR}$ was correlated with the maximum vapor pressure deficit (VPDMAX), shown in Figure 3b, for spring-summer (MAMJJA, $r = 0.55$, $p < 0.05$). While the correlations between $\delta^{18}O_{TR}$ and summer VPDMAX were significant (JJA, $r = 0.44$, $p < 0.05$), non-significant correlations were found with spring VPDMAX (MAM, $r = 0.39$, $p = 0.08$). There were also weaker positive relationships between $\delta^{18}O_{TR}$ and TMIN, and weak negative relationships between $\delta^{18}O_{TR}$ and SNOW during spring (MAM, $r = -0.31$, $p < 0.05$) slightly higher during spring-summer (MAMJJA, $r = -0.33$, $p < 0.05$), as well as between $\delta^{18}O_{TR}$ SNDP (MAM, $r = -0.33$, $p < 0.05$; MAMJJA, $r = -0.34$, $p < 0.05$).

The GHCN TMAX correlation in summer for 1977-2002 was lower ($r = 0.41$, $p < 0.05$) than for the ISD data ($r = 0.48$, $p < 0.05$) likely because most GHCN data were missing for 1993 and 1994. Overall, the strongest correlation with $\delta^{18}O_{TR}$ was found with GHCN TMAX for spring-summer for the whole 1938-2002 period (Figure 3a, Table 2). The strong correlation during this season is related mainly to lower frequency changes in $\delta^{18}O$ and TMAX (Figure 3a). Higher $\delta^{18}O_{TR}$ from 1938 until the late 1950s was associated with warmer temperatures, followed by a decrease in both from 1960 until the early 1970s, and then an increase in $\delta^{18}O_{TR}$ and summer TMAX in the late 1970s, which persisted until the early 2000s.

Based on the strength of spring and summer TMAX controls on $\delta^{18}O_{TR}$, we examined the correlations between $\delta^{18}O_{TR}$ and different gridded climate fields. Figure 4 shows the spatial field correlations between $\delta^{18}O_{TR}$ and seasonal surface temperature anomalies from BEST TMAX, GISTEMP T_{surf} and, for reference, the UDEL precipitation, for the period 1938-2002. For GISTEMP (Figure 4a), there was a positive correlation pattern centered over northern British Columbia during spring-summer (MAMJJA) and extending across most of Canada. The BEST correlation field (Figure 4c) is similar but is smoother and with higher correlations over the study site. For both GISTEMP (Figure 4b) and BEST (Figure 4d), there were no coherent patterns of correlation during autumn-winter (SONDJF), consistent with the analysis performed at the weather station scale. For UDEL precipitation, there were no coherent correlation patterns over the study site for either MAMJJA (Figure 4e) or SONDJF (Figure 4f), showing only weak negative, albeit significant, correlation in continental Canada.

To identify large-scale circulation influences, we also examined $\delta^{18}O_{TR}$ correlation fields for selected variables from the NCEP/NCAR Reanalysis I over 1948-2002 (Figure 5). Temperature correlation maps were similar to GISTEMP and BEST and displayed a coherent region of positive correlation in western Canada during spring-summer (Figure 5a, MAMJJA), but no coherent pattern in autumn-winter (Figure 5b, SONDJF). During either season, there was no coherent correlation pattern between $\delta^{18}O_{TR}$ and precipitation amount (Figure 5c,d). The precipitation amount correlation field was included for completeness, though we note that the NCEP reanalysis precipitation estimates are only weakly constrained by observations (Kalnay et al. 1996), unlike the corresponding UDEL precipitation used in Figure 4e,f. There was also no apparent moisture pathway signature (Figure 5e,f) which would have appeared as a coherent vector field in the vicinity of the study site. No clear correlation pattern was found between $\delta^{18}O_{TR}$ and SLP during either season (Figure 5g,h). There were, however, strong correlations between $\delta^{18}O_{TR}$ and geopotential height at 500 hPa during MAMJJA (Figure 5i), capturing the basic association between warmer temperatures at the site and pronounced high-pressure ridging over western Canada. Individual correlation maps for spring, summer, autumn and winter were similar to the maps using 6-month season definitions for Figure 4 and Figure 5 (Figure S1, S2, S4 and S4). We also compared the NCEP/NCAR 6-month correlation fields (Figure 5) to those for the 20CRv3 reanalysis (Figure S5) for the same period 1948-2002. The region of positive correlation for MAMJJA (Figure S5a) to the southwest of the site is consistent with that for NCEP/NCAR, but it is smaller in its extent and weaker in magnitude, which was also the case for the 500 hPa geopotential height patterns (Figure S5g). The weaker patterns in both cases are presumably due to the 20CRv3 product having far fewer observational constraints. Over the full 1900-2002 length of the $\delta^{18}O_{TR}$ record (Figure S6), there were also positive temperature (Figure S6a) and 500 hPa geopotential height patterns south of the site (Figure S6g), but which were more diffuse in their extent.

3.3. Climate-precipitation δ^{18}O relationships in GISS ModelE2 GCM

Distinct seasonal ModelE2 correlation fields of large-scale circulation features with the modelled precipitation $\delta^{18}O$ over the study site reveal different seasonal influences on source water $\delta^{18}O$ (Figure 6). During spring-summer, the correlation pattern showed a positive relationship between precipitation $\delta^{18}O$ at the study site and temperature over northwestern North America, although with no apparent relationship in eastern Canada (Figure 6a). These features were similar to patterns observed between $\delta^{18}O_{TR}$ and the TMAX field for the GISTEMP (Figure 4a), BEST (Figure 4c) and NCEP reanalysis (Figure 5a) temperature fields. There was also pronounced positive correlation in MAMJJA between modelled precipitation $\delta^{18}O$ and TMAX in the Gulf of Alaska (Figure 6a), seen somewhat in the GISTEMP MAMJJA correlation map with $\delta^{18}O_{TR}$ (Figure 4a). For autumn-winter (SONDJF), there were also pronounced patterns of positive correlation between modelled precipitation $\delta^{18}O$ and TMAX (Figure 6b), unlike the observed relationships between $\delta^{18}O_{TR}$ and TMAX for that season when looking at the study site point scale (Figure 4b). During spring-summer (MAMJJA), there was no apparent relationship between precipitation amount (Figure 6c) or moisture pathway (Figure 6e) and modelled precipitation $\delta^{18}O$ over Tungsten, consistent with the absence of any patterns in the $\delta^{18}O_{TR}$ correlation maps (Figure 5c,e). During autumn-winter (SONDJF), there were more coherent patterns showing a positive relationship between $\delta^{18}O_{TR}$ and precipitation amount in the Gulf of Alaska and negative relationship to the southeast (Figure 6d). During the same season, higher precipitation $\delta^{18}O$ was also associated with southwesterly moisture origin (Figure 6f). For the SLP field, no significant correlation pattern was observed during spring-summer (MAMJJA, Figure 6g), but a strong pattern was found during autumn-winter (SONDJF, Figure 6h) with a negative center over Alaska and the Bering Sea and a positive center over the US Great Plains. The correlation between MAMJJA precipitation $\delta^{18}O$ and 500 hPa geopotential height (Figure 6i) were consistent with that observed for Tungsten $\delta^{18}O_{TR}$ (Figure 5i). The correlation patterns in MAMJJA (Figure 6i) are similar to SONDJF (Figure 6j), but they are stronger in SONDJF.

4. Discussion

In this section, we discuss the signal and stability of the relationship between climate and the tree-ring proxies, the strong imprint of temperature in $\delta^{18}O_{TR}$ and its potential for reconstructing large-scale atmospheric patterns. For the variables considered, the climatic information contained in the TRW was weaker than in the $\delta^{18}O_{TR}$ timeseries, but several significant relationships were identified.

4.1. Instability in the relationship between TRW and climate variables

We found a relatively unstable relationship between climatic and TRW records in some locations. For example, no significant correlation was found between TRW and summer TMAX (June to August, JJA) for the period 1977-2002, while a significant positive correlation was observed over the longer 1938-2002 period with the same dataset (GHCN). This may be related to the divergence-type phenomenon which has been well documented for a number of boreal forest sites (D'Arrigo et al. 2008; and references therein). Local site conditions, recent warming and hydroclimatic trends may also complicate the understanding of the relationship between climate and tree-ring parameters (Gedalof and Smith 2001; Li et al. 2020; Wendler et al. 2017). In the Yukon region for example, almost all of the 111 chronologies from a white spruce network lost their positive relationship with summer temperatures, with one third of them showing negative responses after ~1950 (Morimoto 2015). A weakening of the precipitation signal and subsequent strengthening of temperature sensitivity in white spruce has been recorded in various tree-ring sites from the Alaskan and Canadian interior (Chavardes et al. 2013; Lange et al. 2020). Despite the relative instability of TRW responses in such regions, many TRW records still show strong relationships with local (Jacoby and Cook 1981), as well as larger-scale temperatures and serve for north hemispheric climate reconstructions across a network of sites (D'Arrigo et al. 2014 and references therein).

Considering that cold temperatures in spring may delay the start of the growing season and reduce the period for xylogenesis in northern environments (Rossi et al. 2008), the negative correlation that we found between TRW and spring TMIN (1977-2002) are difficult to interpret. In contrast, the negative correlations between TRW and spring precipitation (1938-2002) may reflect a detrimental effect on growth because spring precipitation falling as snow could delay the start of the growing season. Vaganov et al. (1999) suggested that more abundant snow accumulation may delay snowmelt and induce a delay in cambial activity and a reduction in growth. However, other authors suggested a positive role of spring snowpack on growth related to an increase in moisture availability with higher snowmelt water when the growing season starts in late spring/early summer (Yarie 2008) and/or thermal soil insulation by snow that could enhance growth (Grippa et al. 2005). In moisture-limited sites in western North America forests positive snow-growth relationship has been also reported (Coulthard et al. 2021). In the white spruce forest studied here, a positive effect of larger snowpack on tree-ring growth may be occurring although this relationship was only found in the most recent period (1977-2002).

4.2. Temperature as the dominant signal in the $\delta^{18}O_{TR}$ records

The $\delta^{18}O_{TR}$ relationships identified here were stronger than those for TRW, and broadly consistent with other studies at high-latitude North American sites. In northeastern Canada, Alvarez et al. (2018) found stronger positive correlations between $\delta^{18}O_{TR}$ and TMAX than between $\delta^{18}O_{TR}$ and TMIN. Naulier et al. (2014) found a June-July correlation of $r = 0.55$ ($p < 0.05$) with TMAX and black spruce $\delta^{18}O_{TR}$ over 1949-2005 in Quebec, slightly higher than the correlation of $r = 0.45$ for VPD. Using data from this site combined with a process-based model (MAIDENiso), Lavergne et al. (2017) found that the temperature signal recorded in $\delta^{18}O_{TR}$ more likely reflects the effect of temperature on isotopic enrichment of the leaf water than on the isotopic composition of the source water. Begin et al. (2015) found higher correlations between $\delta^{18}O_{TR}$ and summer VPD than for summer TMAX ($r = 0.64$ versus $r = 0.55$, $p < 0.05$). In Alvarez et al. (2018), $\delta^{18}O_{TR}$ was negatively correlated with river discharge. Similarly, $\delta^{18}O_{TR}$ was negatively correlated with summer precipitation in Naulier et al. (2014) and Begin et al. (2015). We found a negative relationship between precipitation and $\delta^{18}O_{TR}$, but which was weaker and only significant during the combined winter-spring-summer seasonal definition (Table 2). By contrast, Holzkämper et al. (2012) found that $\delta^{18}O_{TR}$ in white spruce was positively correlated with spring temperatures, and negatively correlated with precipitation amount at a site in north-central Canada. In northwestern North America, Porter et al. (2009) found positive relationships between $\delta^{18}O_{TR}$ and early-spring to mid-summer minimum temperatures and summer relative humidity, attributing the former to the temperature dependence of source water $\delta^{18}O$ and the latter to evaporative $\delta^{18}O$ enrichment, and weak negative correlations with April precipitation. This is in agreement with our findings showing that the $\delta^{18}O_{TR}$ series was influenced by temperature variations in spring and summer. While physiological processes have most likely influenced $\delta^{18}O_{TR}$ in summer through evaporative enrichment at leaf level, spring climate also imprints $\delta^{18}O_{TR}$ potentially via temperature effects on precipitation $\delta^{18}O$ signatures (e.g. Treydte et al. 2014).

Snow plays an important role in these latitudes. A possible influence of winter snowpack on $\delta^{18}O_{TR}$ is also suggested by the negative relationships with the snow variables for the 1938-2002 period. Along with a positive correlation observed between $\delta^{18}O_{TR}$ and TMAX, Csank et al. (2016) found a negative correlation between $\delta^{18}O_{TR}$ for a site in southern Alaska and prior winter snow amount. This was consistent with our results, and possibly explained by the effects of snowpack as a moisture source during the growing season. Snow has a lower $\delta^{18}O$ than rain (Kurita et al. 2004), therefore years with greater snow accumulation would contribute to source water in the soil having lower $\delta^{18}O$ (Beria et al. 2018). However, processes operating in the opposite directions could also be taking place, weakening this negative relationship depending on the snow accumulation and residence time of the snow before melting. For example, with more snow, more snowmelt (freeze/unfreeze events), sublimation and other kinetic processes can take place leading to more ^{18}O enrichment (Beria et al. 2018; Ebner et al. 2017).

For all tree-ring and climate parameters considered during the full 1938-2002 period of analysis, $\delta^{18}O_{TR}$ had the highest correlation ($r = 0.67$, $p < 0.05$) with spring and summer TMAX. Since $\delta^{18}O_{TR}$ is influenced by the precipitation $\delta^{18}O$ at the site via soil water, this relationship can be explained, in part, by the large-scale co-variation between temperature and $\delta^{18}O$ precipitation in northern latitudes. This occurs through a Rayleigh distillation of the water vapor that is transported by the air masses (Araguas-Araguas et al. 2000; Gat 1996). Air masses arriving with a colder history will have undergone more rainout, during which the heavier isotopologues (i.e. molecules of a particular element which differ only in the neutron number) will be removed preferentially through fractionation, leading to lower precipitation $\delta^{18}O$ at the sampling site. In addition, during condensation from water vapour to rain, more fractionation of $\delta^{18}O$ occurs under colder conditions than warmer conditions (Clark and Fritz 1997) leading to even more depleted precipitation $\delta^{18}O$ under colder conditions. Therefore, the yearly isotopic signature of precipitation $\delta^{18}O$ is the result of the variation between rainout occurrence due to colder (warmer) air masses that experience more (less) rainout events and rainouts with more (less) ^{18}O

fractionation associated with lower (higher) temperatures during condensation. This is manifested interannually, with lower $\delta^{18}O_{TR}$ in years with lower precipitation $\delta^{18}O$ related to colder upstream conditions (more rainout events and more ^{18}O fractionation during condensation), while higher $\delta^{18}O_{TR}$ in years with higher precipitation $\delta^{18}O$ may be related to warmer upstream conditions (less rainout events and less ^{18}O fractionation during condensation). Note that at high latitudes, there are not strong direct relationships between precipitation amount and precipitation $\delta^{18}O_{TR}$ in the GISS GCM (Schmidt et al., 2007), measurements from the Global Network of Isotopes in Precipitation (Risi et al., 2010) or in an isotopic atmospheric water balance model (Zhang et al. 2015), even when there are positive relationships between temperature and precipitation $\delta^{18}O$. In our study, this was seen by only weak negative correlations with GHCN precipitation during the winter-spring-summer period (Table 2) and a lack of significant correlations between the Tungsten $\delta^{18}O_{TR}$ and both the instrumental precipitation (Fig. 4e,g) and the gridded precipitation fields (Fig. 5c,d). In agreement, our GCM results show a lack of relationship between spring-summer modelled precipitation $\delta^{18}O$ and precipitation and over the Tungsten site (Fig. 6c, d). Note that higher modelled precipitation $\delta^{18}O$ was associated with more precipitation over the Gulf of Alaska and southwesterly moisture transport, which we interpret as primarily as covariation with warmer, more moist air masses arriving from the south to the Gulf of Alaska.

During the 1977-2002 period, $\delta^{18}O_{TR}$ was related to VPDMAX during the annual and combined spring / summer periods. However, the strength of these correlations was mostly driven by summer VPDMAX because non-significant correlations were found in spring alone. Thus, VPD increase may be driven by warmer summers and may induce evaporative ^{18}O enrichment at leaf level during transpiration (Barbour 2007; Gessler et al. 2014). This is consistent with other studies in high-latitude forests of Quebec (e.g. Lavergne et al. 2017). Our GCM results relate to the idealized source water signal unaffected by tree physiological isotopic fractionation. Higher correlation between modelled $\delta^{18}O$ precipitation and temperatures were found in spring compared to summer (Fig. S7a cf. S7b). This indicates that the source water signal is stronger in spring than in summer, illustrated by the GCM diagnosis where physiological enrichment is not present but where other processes such as summer post-condensation exchange weaken the temperature signal. Additionally, as reflected in results from observations with higher correlations between $\delta^{18}O_{TR}$ and temperature in summer than in spring (Fig. S1b cf. Fig. S1a), the temperature signal in the $\delta^{18}O_{TR}$ is higher in summer when both the source water signal and the VPD-induced ^{18}O enrichment at leaf level are present. The strength of the $\delta^{18}O_{TR}$-VPDMAX relationships suggests that annual isotopic measurements in tree rings could be potentially good proxies for reconstructing summer temperature and VPD, but that analyzing earlywood and latewood isotopic measurements independently may be a better option for distinguishing the seasonality effect of source water and VPD in the $\delta^{18}O_{TR}$ signatures at a higher temporal resolution (e.g. Belmecheri et al. 2018; Levesque et al. 2017). However, in the case of the study site, these data are limited by the short length of ISD data over which VPD could be calculated (compared to the longer GHCN records, for example, but which had no humidity records).

4.3. The $\delta^{18}O_{TR}$ records as a proxy for large-scale atmospheric circulation fields

The positive association between $\delta^{18}O_{TR}$ and TMAX timeseries reported is driven by both inter-annual and decadal variations in spring-summer temperature (Figure 3). In this context, can $\delta^{18}O_{TR}$ serve as a proxy for temperature variations or even for large-scale atmospheric circulation fields? The strong $\delta^{18}O_{TR}$ -TMAX relationship was clearly seen regionally in correlation maps with GISTEMP and BEST temperature fields, with areas of higher correlation centered in northwestern North America. This was, in turn, related to a region with positive correlation with 500 hPa geopotential height centered over the study site, which we interpret as a signature of the relationship between high temperature and stronger meridional (southerly) atmospheric flow. This was similar to the patterns seen in the composite relationships between 500 hPa geopotential height and precipitation $\delta^{18}O$ at three sites in central Canada (Birks and Edwards 2009). These relationships between $\delta^{18}O_{TR}$, surface temperature and geopotential height were also seen in those between modelled precipitation $\delta^{18}O$ over the study site, surface temperature and geopotential height in the NASA GISS ModelE2 simulations. In the model simulations, these relationships were seen for both the spring/summer (MAMJJA) and fall/winter (SONDJF), unlike the $\delta^{18}O_{TR}$ for which positive correlations were only seen during the growing season. Similarly, for precipitation amount and moisture transport, coherent positive associations between precipitation $\delta^{18}O$ and southwesterly moisture transport were only seen in model simulations for the SONDJF period; their absence in the $\delta^{18}O_{TR}$ can be explained by weaker circulation features during the spring-summer when trees are growing. The wintertime correlation patterns in SLP and Z_{500} fields are reminiscent of the Pacific North America (PNA) pattern (Barnston and Livezey 1987). Over southern North America, Liu et al. (2014) found a positive to negative dipole correlation pattern between the PNA index and modeled winter precipitation $\delta^{18}O$ (Yoshimura et al. 2008), oriented southeastward from western Canada which is consistent with the spatial pattern observed in Figure 6j This suggests that previous reconstructions of the PNA using tree-ring width records (Liu et al. 2017) could be enhanced with isotopic measurements to further understand hydroclimatic relationships and external forcing over North America throughout the last millennium. Our results also suggest that combining $\delta^{18}O_{TR}$, which is most sensitive to summertime circulation, with other isotopic archives more sensitive to wintertime circulation such as ice cores (Field et al. 2010) have potential for annual or seasonally-varying reconstructions of atmospheric circulation.

4.4. The potential role the Pacific Ocean forcing

Changes in the relationships between climate and both TRW and $\delta^{18}O_{TR}$ over the 1938-2002 period can be in part driven by a regional climate shift in the mid-1970s. After 1977 TRW became insensitive to the previous positive role of summer temperatures, negatively influenced by TMIN and positively by snow depth, while $\delta^{18}O_{TR}$ became more strongly linked to TMAX and insensitive to the previously negative influence of snow depth. We also observed less common variance and higher variability in $\delta^{18}O_{TR}$ among the trees after 1970. The increase in temperature and $\delta^{18}O_{TR}$ during this period is consistent with an abrupt shift towards higher mean annual observed temperature in interior Alaska (Hartmann and Wendler 2005) and a broad range of environmental changes (Ebbesmeyer et al. 1991; Mantua et al. 1997). These were concordant to the well-known regime shift of the Pacific Decadal Oscillation (PDO) in 1976/77 from its negative (cold) to positive (warm) phase (Ebbesmeyer et al. 1991; Mantua et al. 1997; Trenberth and Hurrell 1994) and of the PNA Pattern index to its positive phase (Minobe and Mantua 1999; Overland et al. 1999), both associated with a strengthening of the Aleutian Low. Such apparent readjustment of large-scale mode of climate variability was also seen in $\delta^{18}O_{TR}$ records for the Mackenzie Delta, NWT (Porter et al. 2014), and in $\delta^{18}O$ data from the Mt. Logan ice core (Field et al. 2010). These observations are consistent with the broader regional footprint of TMAX in our $\delta^{18}O_{TR}$ chronology, seen in the correlation patterns with the GISTEMP and BEST gridded temperature products (Figure 4). It is also interesting to note that similar weakness in the strength of the relationship between $\delta^{18}O_{TR}$ and temperatures have also been observed after 1970 in the extra-tropics in Patagonia, South America (Lavergne et al. 2016), reinforcing the hypothesis that our observations may be related to changes in the PDO and its impact in driving inter-hemispheric ocean-atmospheric connections across both of the Western Americas (Villalba et al. 2011).

5. Conclusions

Here, we investigated the potential of tree-ring isotopic and ring-width measurements of white spruce at the boreal forest treeline in the Northwest Territories, Canada to record local to regional climate and reconstruct atmospheric circulation patterns. Among the relationships examined, the strongest was a temperature signal imprinted in $\delta^{18}O_{TR}$ cellulose at the Tungsten site over 1938-2002, likely driven by the precipitation $\delta^{18}O$ signature (i.e. source water). This was seen consistently comparing $\delta^{18}O_{TR}$ with temperature data from different sources, i.e. a weather station, two gridded temperature products, and two reanalyses. The imprint of temperature on $\delta^{18}O_{TR}$ is likely associated to the temperature impact on fractionation processes during the condensation of water vapor to rainwater expected in this high latitude (i.e. colder upstream conditions, more rainout events and more ^{18}O fractionation during condensation leading to lower precipitation $\delta^{18}O$). Evaporative enrichment of ^{18}O at leaf level could also contributing to the final $\delta^{18}O_{TR}$ signature, but just during summer. We also found a weak but significant negative relationship between snow accumulation and $\delta^{18}O_{TR}$ over the 1983-2002 period; a deeper snowpack leads to a greater supply of soil water with lower $\delta^{18}O$ values.

Diagnosis with an isotopically-equipped climate model contributed to our understanding of seasonal differences in the influence of temperature and circulation patterns on the tree-ring data without the influence of tree physiology. No significant relationships were found between the $\delta^{18}O_{TR}$ and reanalysis moisture transport for either fall/winter or spring/summer, but appeared during winter, if unevenly, for the modelled precipitation $\delta^{18}O$ at the sampling site. Our interpretation is that the winter circulation controls on precipitation $\delta^{18}O$ are not strong enough to influence tree uptake of isotopically depleted water during the spring and summer growth season, despite a possible relationship between winter snow depth and $\delta^{18}O_{TR}$.

We conclude that the $\delta^{18}O_{TR}$ records for northwestern Canada reflect the spring-summer atmospheric circulation patterns in this region. The broad consistency of the positive relationships between $\delta^{18}O_{TR}$ and temperature observed in this study and across northern North America demonstrates the potential of using stable oxygen isotopes measured in tree rings for reconstructing temperature, but also other large-scale climate indicators as a novel aspect. Combining the isotopic and other climate signals gleaned from various tree-ring parameters (e.g., MXD, BI) we could produce more robust climate reconstructions. As with dendroclimatological studies from tree-ring width at multiple sites, we therefore expect further gains in reconstructions using a multispecies network (Pederson et al. 2013) of tree-ring isotopic records at regional, continental and eventually hemispheric scales. Forward modeling of tree-ring parameters, as in Lavergne et al. (2017), will further help to understand the relative contributions of 'site-level' processes such as source water uptake and leaf-level processes to better isolate past signals of temperature and moisture variability.

Acknowledgments

This research was supported by a Lamont-Doherty Earth Observatory Climate Center grant and by US National Science Foundation (NSF) grants PLR-1504134, PLR-1603473, AGS-1502150 and OISE-1743738. A.L. was supported by a Marie Sklodowska-Curie Individual Fellowship under the European Union's Horizon 2020 Research and Innovation Programme (grant agreement no: 838739 ECAW-ISO). F.G. was supported by the NSERC Discovery grant RGPIN-2021-03553. We are thankful to Wei Huang from the Stable Isotope Laboratory for their support on isotopic measurements at the Lamont-Doherty Earth Observatory. This is LDEO contribution #

References

AB CED (2019) CooRecorder basics http://www.cybis.se/forfun/dendro/helpcoorecorder7/index.php. (Accessed March 2020).

Alvarez C, Begin C, Savard MM, Dinis L, Marion J, Smirnoff A, Begin Y (2018) Relevance of using whole-ring stable isotopes of black spruce trees in the perspective of climate reconstruction Dendrochronologia 50:64-69 doi:10.1016/j.dendro.2018.05.004

Anchukaitis KJ et al. (2012) Tree-Ring-Reconstructed Summer Temperatures from Northwestern North America during the Last Nine Centuries Journal of Climate 26:3001-3012 doi:10.1175/jcli-d-11-00139.1

Anchukaitis KJ et al. (2017) Last millennium Northern Hemisphere summer temperatures from tree rings: Part II, spatially resolved reconstructions Quaternary Science Reviews 163:1-22 doi:10.1016/j.quascirev.2017.02.020

Andreu-Hayles L, D'Arrigo R, Anchukaitis KJ, Beck P, S. A., Frank D, Goetz S (2011a) Varying boreal forest response to Arctic environmental change at the Firth River, Alaska Environmental Research Letters 6:045503

Andreu-Hayles L et al. (2019) A high yield cellulose extraction system for small whole wood samples and dual measurement of carbon and oxygen stable isotopes Chemical Geology 504:53-65 doi:10.1016/j.chemgeo.2018.09.007

Andreu-Hayles L, Planells O, Gutiérrez E, Muntan E, Helle G, Anchukaitis KJ, Schleser GH (2011b) Long tree-ring chronologies reveal 20th century increases in water-use efficiency but no enhancement of tree growth at five Iberian pine forests Global Change Biology 17:2095-2112 doi:10.1111/j.1365-2486.2010.02373.x

Andreu-Hayles L et al. (2017) 400 Years of summer hydroclimate from stable isotopes in Iberian trees Climate Dynamics 49:143-161 doi:10.1007/s00382-016-3332-z

Araguas-Araguas L, Froehlich K, Rozanski K (2000) Deuterium and oxygen-18 isotope composition of precipitation and atmospheric moisture Hydrol Process 14:1341-1355 doi:10.1002/1099-1085(20000615)14:8<1341::Aid-hyp983>3.0.Co;2-z

Balting DF et al. (2021) Large-scale climate signals of a European oxygen isotope network from tree rings Clim Past 17:1005-1023 doi:10.5194/cp-17-1005-2021

Barber VA, Juday GP, Finney BP (2000) Reduced growth of Alaskan white spruce in the twentieth century from temperature-induced drought stress Nature 405:668-673

Barbeta A et al. (2020) Evidence for distinct isotopic composition of sap and tissue water in tree stems: consequences for plant water source identification bioRxiv:2020.2006.2018.160002 doi:10.1101/2020.06.18.160002

Barbour MM (2007) Stable oxygen isotope composition of plant tissue: a review Functional Plant Biology 34:83-94 doi:http://dx.doi.org/10.1071/FP06228

Barnston AG, Livezey RE (1987) Classification, Seasonality and Persistence of Low-Frequency Atmospheric Circulation Patterns Monthly Weather Review 115:1083-1126 doi:10.1175/1520-0493(1987)115<1083:csapol>2.0.co;2

Begin C, Gingras M, Savard MM, Marion J, Nicault A, Begin Y (2015) Assessing tree-ring carbon and oxygen stable isotopes for climate reconstruction in the Canadian northeastern boreal forest Palaeogeography Palaeoclimatology Palaeoecology 423:91-101 doi:10.1016/j.palaeo.2015.01.021

Belmecheri S, Wright WE, Szejner P, Morino KA, Monson RK (2018) Carbon and oxygen isotope fractionations in tree rings reveal interactions between cambial phenology and seasonal climate Plant Cell and Environment 41:2758-2772 doi:10.1111/pce.13401

Beria H, Larsen JR, Ceperley NC, Michelon A, Vennemann T, Schaefli B (2018) Understanding snow hydrological processes through the lens of stable water isotopes WIREs Water 5:e1311 doi:https://doi.org/10.1002/wat2.1311

Birks SJ, Edwards TWD (2009) Atmospheric circulation controls on precipitation isotope-climate relations in western Canada Tellus Series B-Chemical and Physical Meteorology 61:566-576 doi:10.1111/j.1600-0889.2009.00423.x

Briffa KR, Osborn TJ, Schweingruber FH (2004) Large-scale temperature inferences from tree rings: a review Global and Planetary Change 40:11-26 doi:10.1016/s0921-8181(03)00095-x

Brigode P, Brissette F, Nicault A, Perreault L, Kuentz A, Mathevet T, Gailhard J (2016) Streamflow variability over the 1881-2011 period in northern Quebec: comparison of hydrological reconstructions based on tree rings and geopotential height field reanalysis Climate of the Past 12:1785-1804 doi:10.5194/cp-12-1785-2016

Brinkmann N, Seeger S, Weiler M, Buchmann N, Eugster W, Kahmen A (2018) Employing stable isotopes to determine the residence times of soil water and the temporal origin of water taken up by Fagus sylvatica and Picea abies in a temperate forest New Phytologist 219:1300-1313 doi:10.1111/nph.15255

Cernusak LA et al. (2016) Stable isotopes in leaf water of terrestrial plants Plant Cell and Environment 39:1087-1102 doi:10.1111/pce.12703

Chavardes RD, Daniels LD, Waeber PO, Innes JL, Nitschke CR (2013) Unstable climate-growth relations for white spruce in southwest Yukon, Canada Climatic Change 116:593-611 doi:10.1007/s10584-012-0503-8

Clark I, Fritz P (1997) Environmental Isotopes in Hydrogeology.

Cook ER, Kairiukstis L (1990) Methods of Dendrochronology in Applications in the Environmental Sciences Kluwer, Dordrecht, 394 pp.,

Cook ER, Peters K (1981) The smoothing spline: a new approach to standardizing forest interior tree-ring width series for dendroclimatic studies Tree-Ring Bulletin 41:45-53

Cook ER, Peters K (1997) Calculating unbiased tree-ring indices for the study of climatic and environmental change Holocene 7:359–368

Coulthard BL, Anchukaitis KJ, Pederson GT, Cook E, Littell J, Smith DJ (2021) Snowpack signals in North American tree rings Environmental Research Letters 16:034037 doi:10.1088/1748-9326/abd5de

Csank AZ, Fortier D, Leavitt SW (2013) Annually resolved temperature reconstructions from a late Pliocene–early Pleistocene polar forest on Bylot Island, Canada Palaeogeography, Palaeoclimatology, Palaeoecology 369:313-322 doi:http://dx.doi.org/10.1016/j.palaeo.2012.10.040

Csank AZ, Miller AE, Sherriff RL, Berg EE, Welker JM (2016) Tree-ring isotopes reveal drought sensitivity in trees killed by spruce beetle outbreaks in south-central Alaska Ecological Applications 26:2001-2020 doi:10.1002/eap.1365

D'Arrigo R et al. (2014) Temperature Reconstructions for the Northern Hemisphere. In: Dendroclimatic Studies: Tree Growth and Climate Change in Northern Forests, vol 67. pp 23-35

D'Arrigo R, Villalba R, Wiles G (2001) Tree-ring estimates of Pacific decadal climate variability Climate Dynamics 18:219-224 doi:10.1007/s003820100177

D'Arrigo R, Wilson R, Liepert B, Cherubini P (2008) On the 'Divergence Problem' in Northern Forests: A review of the tree-ring evidence and possible causes Global and Planetary Change 60:289-305 doi:10.1016/j.gloplacha.2007.03.004

Dansgaard W (1964) STABLE ISOTOPES IN PRECIPITATION Tellus 16:436-468

Durre I, Menne MJ, Gleason BE, Houston TG, Vose RS (2010) Comprehensive Automated Quality Assurance of Daily Surface Observations Journal of Applied Meteorology and Climatology 49:1615-1633 doi:10.1175/2010jamc2375.1

Ebbesmeyer CC, Cayan DR, Milan DR, Nichols FH, Peterson DH, Redmond KT (1991) 1976 step in the Pacific climate: forty environmental changes between 1968–1975 and 1977–1984. p. 115–126. In Proceedings of the 7th Annual Climate (PACLIM) Workshop, April 1990, ed. by J. L. Betancourt and V. L. Tharp, California Department of Water Resources, Interagency Ecological Studies Program Technical Report 26.

Ebner PP, Steen-Larsen HC, Stenni B, Schneebeli M, Steinfeld A (2017) Experimental observation of transient δ18O interaction between snow and advective airflow under various temperature gradient conditions The Cryosphere 11:1733-1743 doi:10.5194/tc-11-1733-2017

Field RD, Moore GWK, Holdsworth G, Schmidt GA (2010) A GCM-based analysis of circulation controls on delta O-18 in the southwest Yukon, Canada: Implications for climate reconstructions in the region Geophysical Research Letters 37 doi:10.1029/2009gl041408

Gaglioti BV et al. (2019) Traumatic Resin Ducts in Alaska Mountain Hemlock Trees Provide a New Proxy for Winter Storminess Journal of Geophysical Research-Biogeosciences 124:1923-1938 doi:10.1029/2018jg004849

Gat JR (1996) Oxygen and hydrogen isotopes in the hydrologic cycle Annu Rev Earth Planet Sci 24:225-262 doi:10.1146/annurev.earth.24.1.225

Gedalof Z, Smith DJ (2001) Interdecadal climate variability and regime-scale shifts in Pacific North America Geophysical Research Letters 28:1515-1518 doi:10.1029/2000gl011779

Gennaretti F, Huard D, Naulier M, Savard M, Begin C, Arseneault D, Guiot J (2017) Bayesian multiproxy temperature reconstruction with black spruce ring widths and stable isotopes from the northern Quebec taiga Climate Dynamics 49:4107-4119 doi:10.1007/s00382-017-3565-5

Gessler A, Pedro Ferrio J, Hommel R, Treydte K, Werner RA, Monson RK (2014) Stable isotopes in tree rings: towards a mechanistic understanding of isotope fractionation and mixing processes from the leaves to the wood Tree Physiol 34:796-818 doi:10.1093/treephys/tpu040

Grippa M, Kergoat L, Le Toan T, Mognard NM, Delbart N, L'Hermitte J, Vicente-Serrano SM (2005) The impact of snow depth and snowmelt on the vegetation variability over central Siberia Geophysical Research Letters 32 doi:https://doi.org/10.1029/2005GL024286

Hartmann B, Wendler G (2005) The significance of the 1976 Pacific climate shift in the climatology of Alaska Journal of Climate 18:4824-4839 doi:10.1175/jcli3532.1

Holzkamper S, Tillman PK, Kuhry P, Esper J (2012) Comparison of stable carbon and oxygen isotopes in Picea glauca tree rings and Sphagnum fuscum moss remains from subarctic Canada Quaternary Research 78:295-302 doi:10.1016/j.yqres.2012.05.014

Jacoby GC, Cook ER (1981) PAST TEMPERATURE-VARIATIONS INFERRED FROM A 400-YEAR TREE-RING CHRONOLOGY FROM YUKON-TERRITORY, CANADA Arctic and Alpine Research 13:409-418 doi:10.2307/1551051

Kalnay E et al. (1996) The NCEP/NCAR 40-year reanalysis project Bulletin of the American Meteorological Society 77:437-471 doi:10.1175/1520-0477(1996)077<0437:tnyrp>2.0.co;2

Kurita N, Yoshida N, Inoue G, Chayanova EA (2004) Modern isotope climatology of Russia: A first assessment Journal of Geophysical Research-Atmospheres 109 doi:10.1029/2003jd003404

Lange J, Carrer M, Pisaric MFJ, Porter TJ, Seo J-W, Trouillier M, Wilmking M (2020) Moisture-driven shift in the climate sensitivity of white spruce xylem anatomical traits is coupled to large-scale oscillation patterns across northern treeline in northwest North America Global Change Biology 26:1842-1856 doi:10.1111/gcb.14947

Lavergne A, Daux V, Villalba R, Pierre M, Stievenard M, Vimeux F, Srur AM (2016) Are the oxygen isotopic compositions of Fitzroya cupressoides and Nothofagus pumilio cellulose promising proxies for climate reconstructions in northern Patagonia? Journal of Geophysical Research-Biogeosciences 121:767-776 doi:10.1002/2015jg003260

Lavergne A et al. (2017) Modelling tree ring cellulose delta O-18 variations in two temperature-sensitive tree species from North and South America Clim Past 13:1515-1526 doi:10.5194/cp-13-1515-2017

Legates DR, Willmott CJ (1990) MEAN SEASONAL AND SPATIAL VARIABILITY IN GAUGE-CORRECTED, GLOBAL PRECIPITATION Int J Climatol 10:111-127 doi:10.1002/joc.3370100202

Lenssen NJL, Schmidt GA, Hansen JE, Menne MJ, Persin A, Ruedy R, Zyss D (2019) Improvements in the GISTEMP Uncertainty Model Journal of Geophysical Research-Atmospheres 124:6307-6326 doi:10.1029/2018jd029522

Levesque M, Andreu-Hayles L, Pederson N (2017) Water availability drives gas exchange and growth of trees in northeastern US, not elevated CO2 and reduced acid deposition Scientific Reports 7:9 doi:10.1038/srep46158

Li SJ et al. (2020) The Pacific Decadal Oscillation less predictable under greenhouse warming Nature Climate Change 10:30-+ doi:10.1038/s41558-019-0663-x

Liu ZF, Tang YL, Jian ZM, Poulsen CJ, Welker JM, Bowen GJ (2017) Pacific North American circulation pattern links external forcing and North American hydroclimatic change over the past millennium Proceedings of the National Academy of Sciences of the United States of America 114:3340-3345 doi:10.1073/pnas.1618201114

Mantua NJ, Hare SR, Zhang Y, Wallace JM, Francis RC (1997) A Pacific interdecadal climate oscillation with impacts on salmon production Bulletin of the American Meteorological Society 78:1069-1079

McCarroll D, Loader NJ (2004) Stable isotopes in tree rings Quaternary Research Reviews 23:771-801

Minobe S, Mantua N (1999) Interdecadal modulation of interannual atmospheric and oceanic variability over the North Pacific Progress in Oceanography 43:163-192 doi:http://dx.doi.org/10.1016/S0079-6611(99)00008-7

Morimoto DS (2015) Dendroclimatic Studies of White Spruce in the Yukon Territory, Canada, Electronic Thesis and Dissertation Repository. 2991. https://ir.lib.uwo.ca/etd/2991

Naulier M et al. (2015) A millennial summer temperature reconstruction for northeastern Canada using oxygen isotopes in subfossil trees Clim Past 11:1153-1164 doi:10.5194/cp-11-1153-2015

Naulier M, Savard MM, Begin C, Marion J, Arseneault D, Begin Y (2014) Carbon and oxygen isotopes of lakeshore black spruce trees in northeastern Canada as proxies for climatic reconstruction Chemical Geology 374:37-43 doi:10.1016/j.chemgeo.2014.02.031

Overland JE, Adams JM, Bond NA (1999) Decadal Variability of the Aleutian Low and Its Relation to High-Latitude Circulation Journal of Climate 12:1542-1548 doi:10.1175/1520-0442(1999)012<1542:Dvotal>2.0.Co;2

Pederson N et al. (2013) Is an Epic Pluvial Masking the Water Insecurity of the Greater New York City Region? Journal of Climate 26:1339-1354 doi:10.1175/jcli-d-11-00723.1

Porter TJ et al. (2014) Spring-summer temperatures since AD 1780 reconstructed from stable oxygen isotope ratios in white spruce tree-rings from the Mackenzie Delta, northwestern Canada Climate Dynamics 42:771-785 doi:10.1007/s00382-013-1674-3

Porter TJ, Pisaric MFJ, Kokelj SV, Edwards TWD (2009) Climatic signals in delta C-13 and delta O-18 of Tree-rings from White Spruce in the Mackenzie Delta Region, Northern Canada Arctic Antarctic and Alpine Research 41:497-505 doi:10.1657/1938-4246-41.4.497

Rohde R et al. (2013) A New Estimate of the Average Earth Surface Land Temperature Spanning 1753 to 2011 Geoinformatics & Geostatistics: An Overview doi:10.4172/2327-4581.1000101

Schmidt GA et al. (2014) Configuration and assessment of the GISS ModelE2 contributions to the CMIP5 archive Journal of Advances in Modeling Earth Systems 6:141-184 doi:10.1002/2013ms000265

Slivinski LC et al. (2019) Towards a more reliable historical reanalysis: Improvements for version 3 of the Twentieth Century Reanalysis system Quarterly Journal of the Royal Meteorological Society 145:2876-2908 doi:https://doi.org/10.1002/qj.3598

Smith A, Lott N, Vose R (2011) The Integrated Surface Database Recent Developments and Partnerships Bulletin of the American Meteorological Society 92:704-708 doi:10.1175/2011bams3015.1

Stokes M, Smiley T (1968) An introduction to tree-ring dating:University of Chicago Press, Chicago, 73 pp.

Szejner P et al. (2016) Latitudinal gradients in tree ring stable carbon and oxygen isotopes reveal differential climate influences of the North American Monsoon System Journal of Geophysical Research-Biogeosciences 121:1978-1991 doi:10.1002/2016jg003460

Trenberth KE, Hurrell JW (1994) Decadal atmosphere-ocean variations in the Pacific Climate Dynamics 9:303-319 doi:10.1007/bf00204745

Treydte K et al. (2014) Seasonal transfer of oxygen isotopes from precipitation and soil to the tree ring: source water versus needle water enrichment New Phytologist 202:772-783 doi:10.1111/nph.12741

Villalba R et al. (2011) Dendroclimatology from Regional to Continental Scales: Understanding Regional Processes to Reconstruct Large-Scale Climatic Variations Across the Western Americas. In: Hughes MK, Swetnam TW, Diaz HF (eds) Dendroclimatology, vol 11. Developments in Paleoenvironmental Research. Springer Netherlands, pp 175-227. doi:10.1007/978-1-4020-5725-0_7

Wendler G, Gordon T, Stuefer M (2017) On the Precipitation and Precipitation Change in Alaska Atmosphere 8 doi:10.3390/atmos8120253

Wilson R et al. (2019) Improved dendroclimatic calibration using blue intensity in the southern Yukon Holocene:14 doi:10.1177/0959683619862037

Wilson R et al. (2016) Last millennium northern hemisphere summer temperatures from tree rings: Part I: The long term context Quaternary Science Reviews 134:1-18 doi:10.1016/j.quascirev.2015.12.005

Wilson R, D'Arrigo R, Andreu-Hayles L, Oelkers R, Wiles G, Anchukaitis K, Davi N (2017) Experiments based on blue intensity for reconstructing North Pacific temperatures along the Gulf of Alaska Clim Past 13:1007-1022 doi:http://dx.doi.org/10.5194/cp-13-1007-2017

Wilson RJS, Luckman BH (2003) Dendroclimatic reconstruction of maximum summer temperatures from upper treeline sites in Interior British Columbia, Canada Holocene 13:851-861 doi:10.1191/0959683603hl663rp

Yarie J (2008) Effects of moisture limitation on tree growth in upland and floodplain forest ecosystems in interior Alaska For Ecol Manage 256:1055-1063 doi:10.1016/j.foreco.2008.06.022

Zhang XP, Guan HD, Zhang XZ, Wu HW, Li G, Huang YM (2015) Simulation of stable water isotopic composition in the atmosphere using an isotopic Atmospheric Water Balance Model Int J Climatol 35:846-859 doi:10.1002/joc.4019

Table 1. Pearson's correlation coefficients (*r*) between Tungsten annual tree-ring width (TRW) residual and seasonal "Watson Lake A" maximum temperature (TMAX), minimum temperature (TMIN), and maximum vapor pressure deficit (VPDMAX) from the Integrated Surface Database (ISD) over 1977-2002, and TMAX, minimum temperature (TMIN), precipitation (PREC), snowfall (SNOW), and snow depth (SNDP) from the Global Historical Climate Network (GHCN) during 1977-2002 and 1938-2002. The seasons abbreviations are according to the first letter of the month, with SONDJFMAMJJA and DFJMAMJJA beginning in the previous year. Only correlations with $p<0.05$ are shown. SNDP data were available only over 1956-2002.

	ISD 1977-2002			GHCN 1977-2002					GHCN 1938-2002				
Season	TMAX	TMIN	VPDMAX	TMAX	TMIN	PREC	SNOW	SNDP	TMAX	TMIN	PREC	SNOW	SNDP
JFMAMJJASOND								0.44			-0.31		
MAMJJA								0.62			-0.32		
SONDJF													
MAM		-0.48			-0.49			0.64			-0.36		
JJA									0.34				
SON													
DJF													
DJFMAMJJA		-0.45						0.58			-0.39		

Table 2. Same as Table 1, but for annual tree ring $\delta^{18}O$ z-scores.

	ISD 1977-2002			GHCN 1977-2002					GHCN 1938-2002				
Season	TMAX	TMIN	VPDMAX	TMAX	TMIN	PREC	SNOW	SNDP	TMAX	TMIN	PREC	SNOW	SNDP
JFMAMJJASOND			0.55						0.42	0.30			
MAMJJA	0.49		0.55						0.67	0.51		-0.33	-0.34
SONDJF													
MAM									0.37	0.28		-0.31	-0.33
JJA	0.48	0.50	0.44	0.41					0.51	0.27			
SON													
DJF													
DJFMAMJJA			0.55						0.52	0.43	-0.29	-0.33	

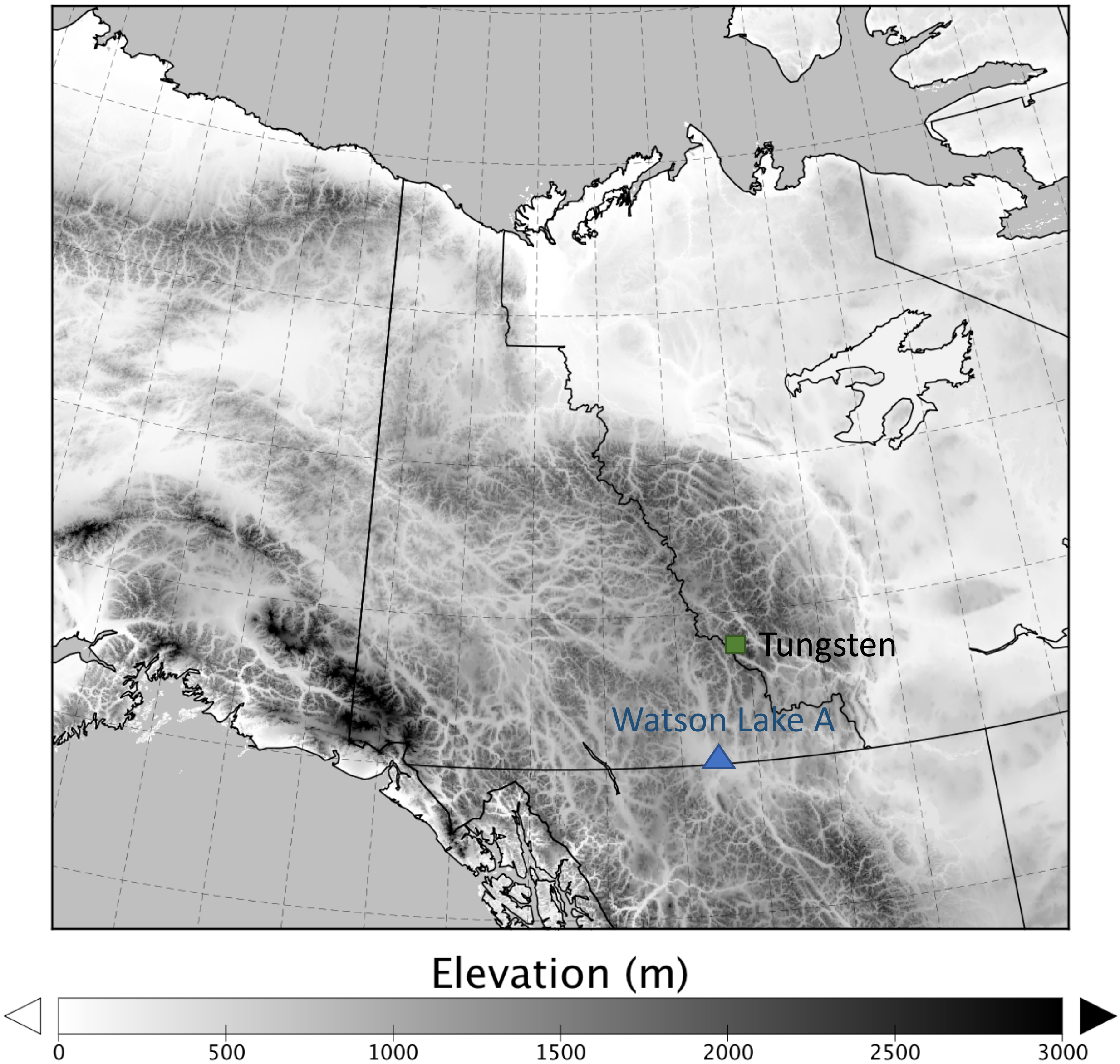

Figure 1. Location of the tree-ring chronology at Tungsten (61.98ºN; 128.25ºW) and the Watson Lake Global Historical Climatological Network (GHCN) weather station (60.117N, 128.817W).

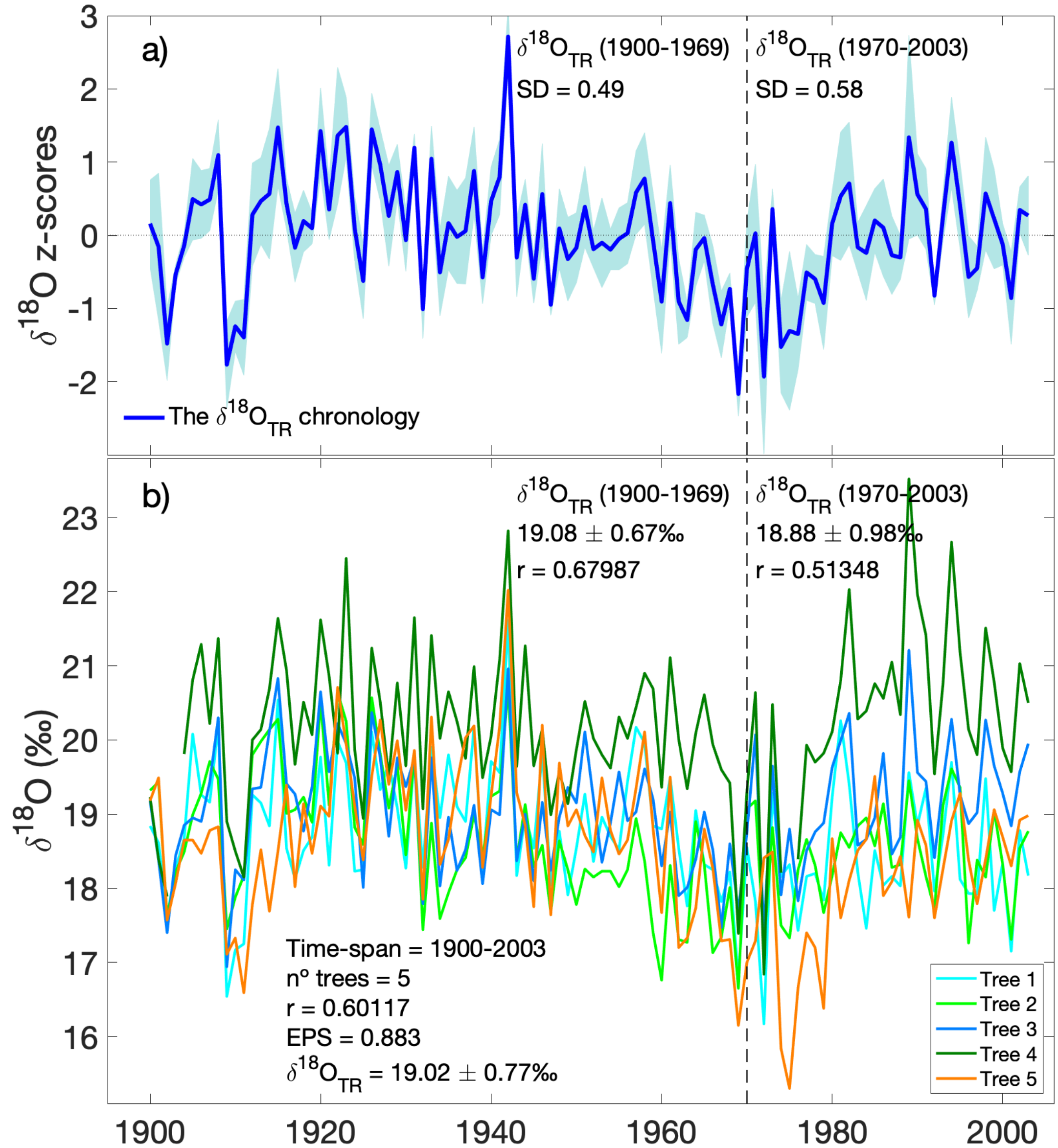

Figure 2. (a) The $\delta^{18}O_{TR}$ chronology for the Tungsten site which was calculated averaging the z-scores of the $\delta^{18}O_{TR}$ individual timeseries. (b) The raw $\delta^{18}O_{TR}$ individual timeseries (r = averaged Pearson correlation coefficient between the five trees; EPS = Expressed Population Signal).

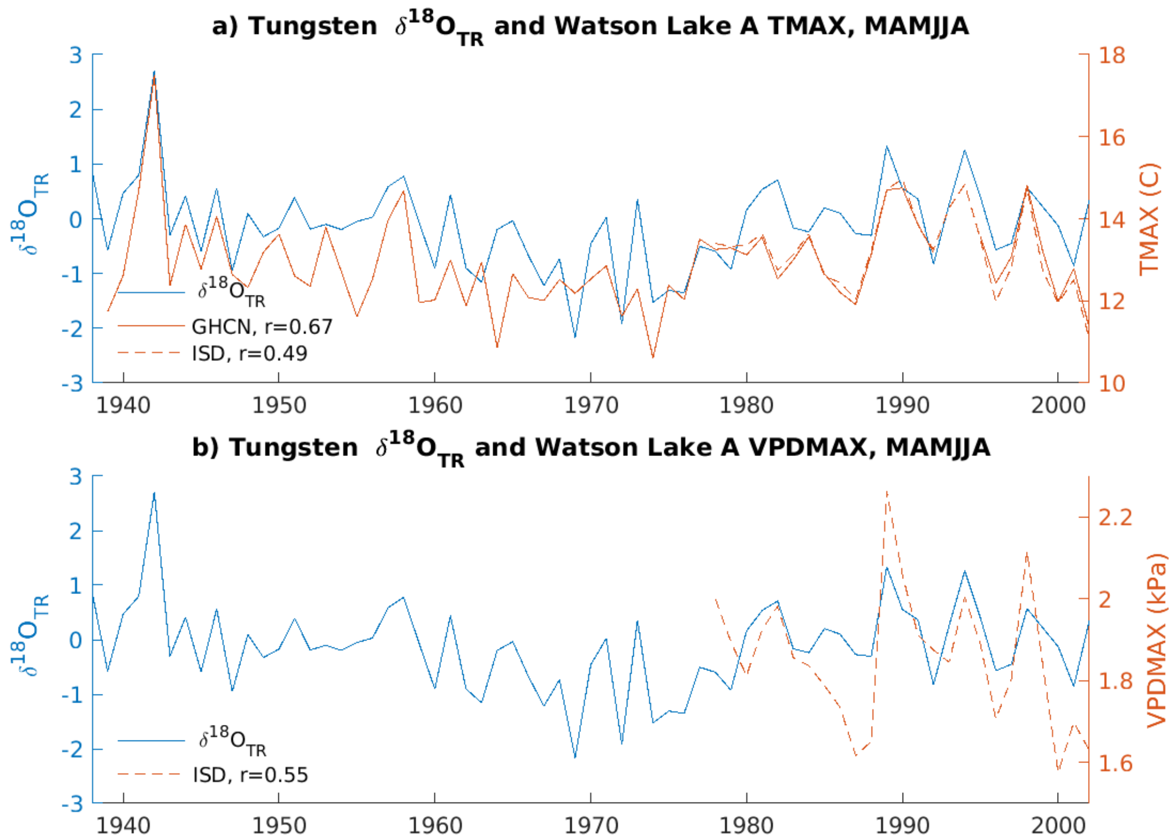

Figure 3. a) The tree-ring (TR) δ^{18}O chronology (z-scores, blue) and average spring-summer (MAMJJA) TMAX at GHCN and ISD Watson Lake A weather station (bold and dashed orange lines, respectively), and b) The TR δ^{18}O chronology (z-scores, blue) and average spring-summer VPDMAX from ISD at the same station (dashed orange line). The r indicates the Pearson correlation coefficient between the $\delta^{18}O_{TR}$ chronology and the climate timeseries.

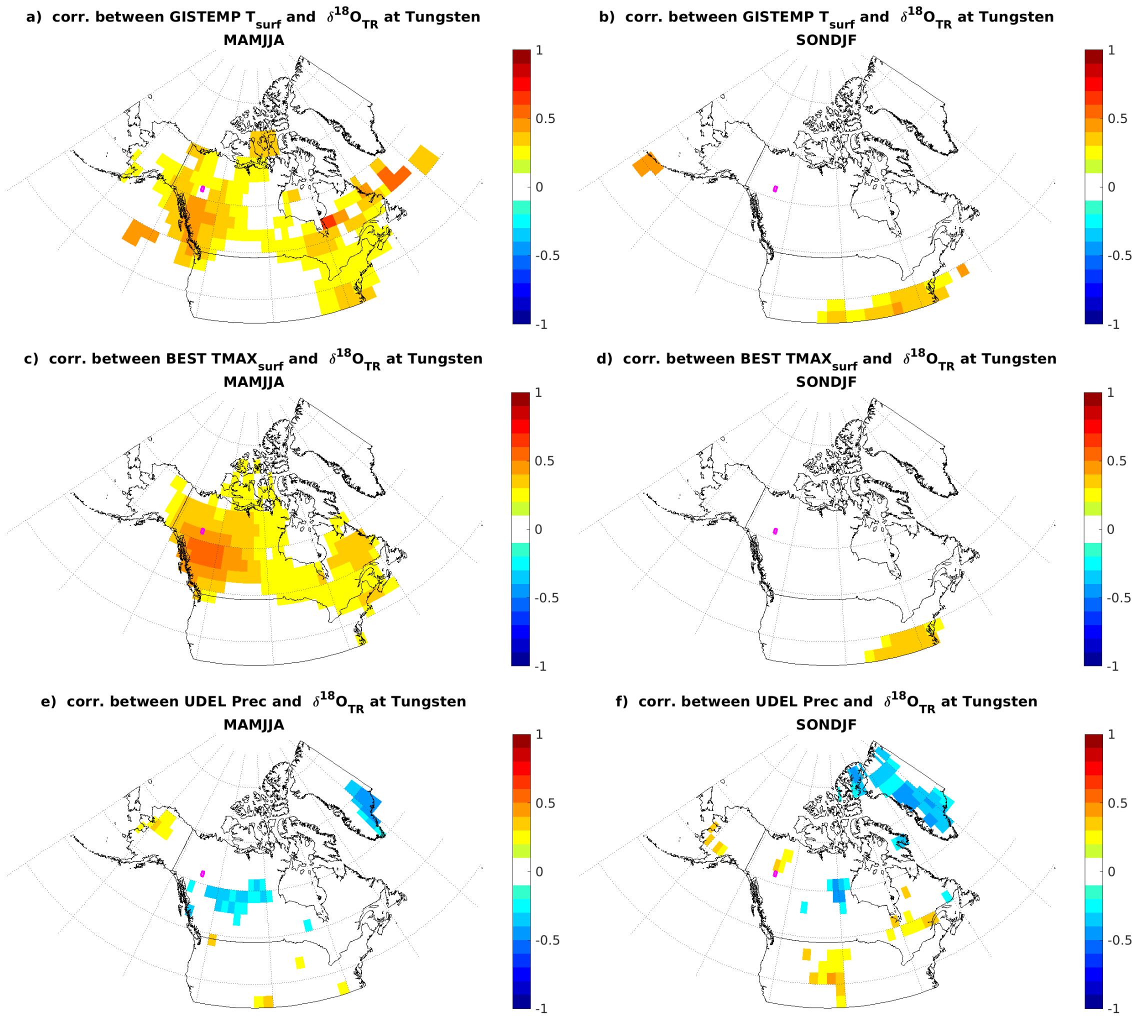

Figure 4. Spatial field correlations between annual tree-ring (TR) $\delta^{18}O$ and GISTEMP surface temperature anomaly (top), BEST maximum surface temperature (middle), and University of Delaware (UDEL) precipitation (bottom) over land for spring-summer (March-August, MAMJJA, left) and autumn-winter (September of the previous year to February (SONDJF, right), over 1938-2002. Correlations with p-values < 0.05 have been excluded. The location of the Tungsten site is shown by the small magenta box.

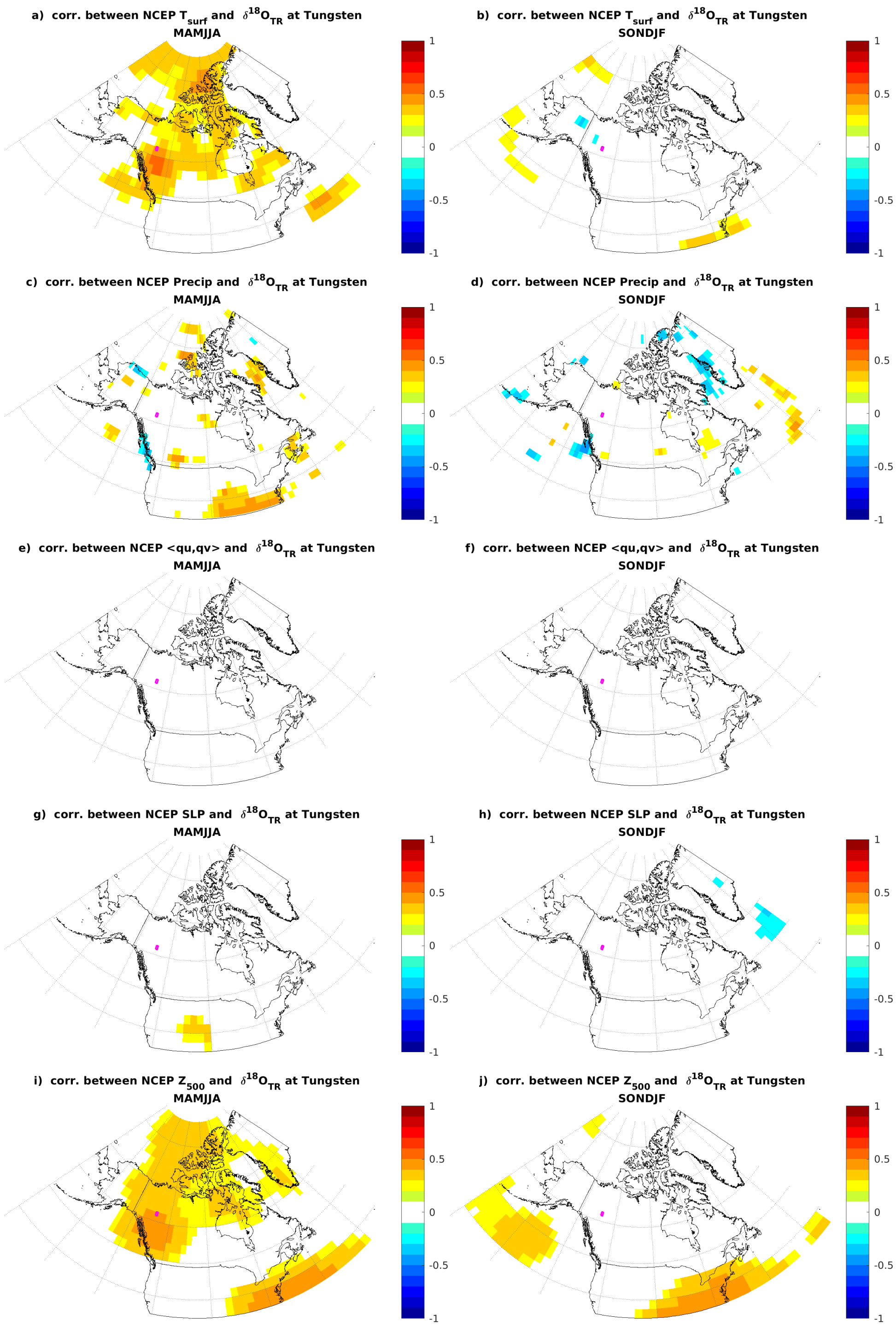

Figure 5. Spatial field correlations between annual tree-ring (TR) δ^{18}O and NCEP surface temperature (T_{surf}), precipitation (Precip), moisture transport at 500 hPa (<qu,qv>), sea-level pressure (SLP), and geopotential height at 500 hPa (Z_{500}) for spring-summer (March-August, MAMJJA, left) and autumn-winter (September-February, SONDJF, right), over 1948-2012. Correlations with p-values < 0.05 have been excluded.

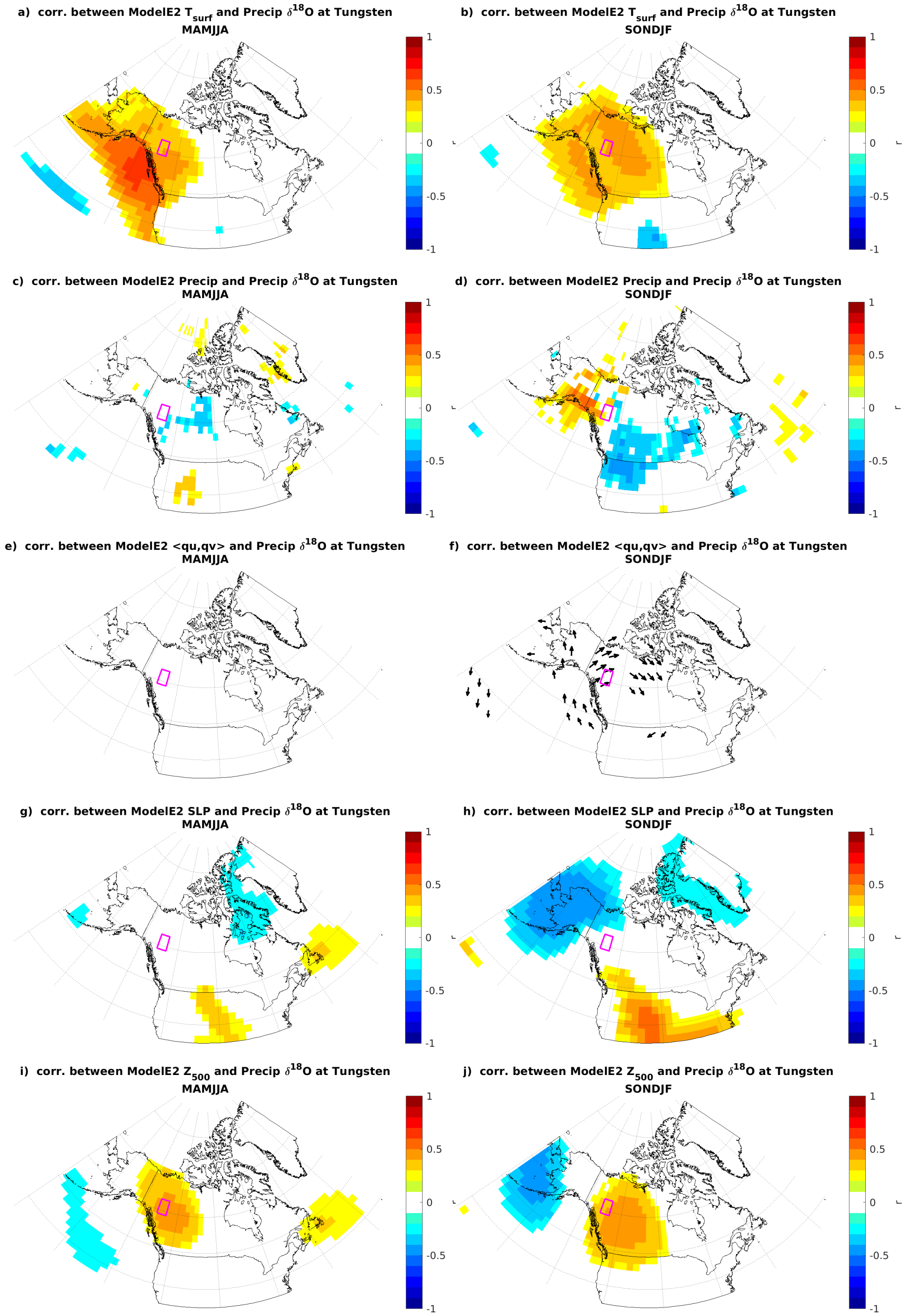

Figure 6. Spatial field correlations between annual ModelE2 precipitation δ^{18}O over the Tungsten site and surface temperature (T_{surf}), precipitation (Precip), moisture transport at 500 hPa (<qu,qv>), sea-level pressure (SLP), and geopotential height at 500 hPa (Z_{500}) for spring-summer (March-August, MAMJJA, left) and autumn-winter (September-February, SONDJF, right), over 1952-2012. Correlations with p-values < 0.05 have been excluded.